Analytical signal analysis of strange nonchaotic dynamics

Kopal Gupta,* Awadhesh Prasad,† and Harinder P. Singh‡
Department of Physics and Astrophysics, University of Delhi, Delhi 110007, India

Ramakrishna Ramaswamy§
School of Physical Sciences, Jawaharlal Nehru University, New Delhi 110067, India

(Received 31 January 2008; published 25 April 2008)

We apply an analytical signal analysis to strange nonchaotic dynamics. Through this technique it is possible to obtain the spectrum of instantaneous intrinsic mode frequencies that are present in a given signal. We find that the second-mode frequency and its variance are good order parameters for dynamical transitions from quasiperiodic tori to strange nonchaotic attractors (SNAs) and from SNAs to chaotic attractors. Phase fluctuation analysis shows that SNAs and chaotic attractors behave identically within short time windows as a consequence of local instabilities in the dynamics. In longer time windows, however, the globally stable character of SNAs becomes apparent. This methodology can be of great utility in the analysis of experimental time series, and representative applications are made to signals obtained from Rössler and Duffing oscillators.

DOI: 10.1103/PhysRevE.77.046220 PACS number(s): 05.45.Tp, 05.45.Pq, 05.45.Ac, 05.40.Jc

I. INTRODUCTION

In quasiperiodically driven nonlinear dynamical systems, strange nonchaotic dynamics [1,2] usually occurs as transitional behavior between regimes of (strange) chaotic motion and quasiperiodic tori: namely, nonchaotic and nonstrange behavior [3]. From the time when such attractors were explicitly described [4], a number of theoretical studies have addressed different aspects such as quantitative measures to characterize them and the different bifurcations that create strange nonchaotic attractors (SNAs) [5–7].

There are some subtleties involved since SNAs are geometrically strange, typically fractal, objects on which the largest nontrivial Lyapunov exponent is nonpositive. Some structural features are thus shared with strange chaotic attractors while some dynamical features are shared with regular orbits. The number of experimental studies where SNAs have definitively been identified are, however, few [8,9]. Detecting the transition from the regular orbits—tori—to SNAs is relatively easy via any measure which probes the geometrical structure of the attractors. For example, the fractal dimension is integral for tori, while it has a noninteger value for SNAs. Fluctuations in finite-time Lyapunov exponents also capture the geometric properties of attractors and have been used to detect the transition from tori to SNAs [6,10]. The transition from SNAs to chaos is, likewise, easily detected through the Lyapunov exponent itself which crosses zero, changing from negative to positive.

Detecting the nature of the motion from experimentally measured time series can be difficult. Obtaining a bound on the fractal dimension is possible, but this does not differentiate between chaotic and nonchaotic attractors. On the other hand, simple methods usually are not able to accurately estimate a negative Lyapunov exponent from an aperiodic time series. Transitions in the dynamics, particularly from SNAs to chaos, are thus quite difficult to detect. Earlier studies [11] have pointed out that the Lyapunov exponent increases linearly and its fluctuations show a small linear jump at the transition [6]. More recently, Ngamga *et al.* [12] have used recurrence analysis to identify the transitions. However, this method is nonadaptive, in the sense that it is necessary to *preset* some parameters prior to performing the analysis with the time-series data.

In this paper we use analytical signal analysis (ASA) [13] to address some of these issues. The analytic signal analysis was first developed by Gabor [14] in his study of optical holography in order to define a complex signal with a clear physical meaning. We demonstrate here that the ASA—and in particular, measures based on the second largest frequency of the signal and its variance—is especially suited to detection of the transition from SNAs to chaos. Further, we also study the phase fluctuations of the signal [15] which also help to differentiate between SNAs and chaotic attractors by helping identify features corresponding to local instability and global stability.

A major motivation for this work is to develop tools for detection of SNAs from time-series data alone. An outline of the ASA method is first discussed in the following section, Sec. II. This is then applied to the model Rössler and Duffing oscillator systems in Sec. III. We discuss the results in Sec. IV. The paper concludes with a summary in Sec. V.

II. ANALYTICAL SIGNAL ANALYSIS

We briefly recall the essential features of the analytical signal analysis proposed by Gabor [14] that has proven to be very useful in the analysis of signals that are not periodic [11,15]. Given a signal $x(t)$, the amplitude A and phase ϕ of the so-called analytical signal $\psi(t)$ is determined through the equation

$$\psi(t) = x(t) + i\tilde{x}(t) = A(t)e^{i\phi(t)}, \tag{1}$$

with

*kopal@physics.du.ac.in
†awadhesh@physics.du.ac.in
‡hpsingh@physics.du.ac.in
§r.ramaswamy@mail.jnu.ac.in

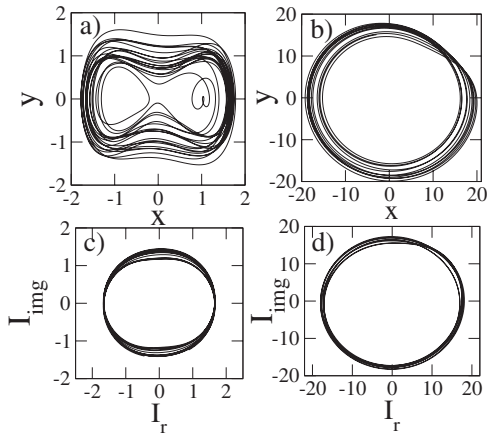

FIG. 1. Plot of x vs y for the forced (a) Duffing oscillator at $R=0.39$ and (b) Rössler system at $\alpha=0.05$. Plot of I_r vs I_{img} for the first IMF obtained by EMD of the trajectories in the (c) forced Duffing and (d) Rössler systems, respectively.

$$\tilde{x}(t) = \frac{1}{\pi}\text{P.V.}\left(\int_{-\infty}^{\infty}\frac{x(t')}{t-t'}dt'\right), \tag{2}$$

"P.V." denoting the Cauchy principal value in the above Hilbert transform. The quantities

$$A(t) = \sqrt{x(t)^2 + \tilde{x}(t)^2}$$

and

$$\phi(t) = \tan^{-1}[\tilde{x}(t)/x(t)]$$

define the amplitude and phase of the analytical signal.

When $x(t)$ is aperiodic [see Figs. 1(a) and 1(b)], the rate of rotation about a fixed point of its analytical signal—namely, the frequency $\omega(t)=\dot{\phi}(t)$—is not constant. Indeed, the nature of its variation reveals much about the nature of the dynamics. Thus, it is necessary to subject the signal to further analysis. A method that has been gaining increasing attention [11,15,16] is the so-called empirical mode decomposition (EMD) [13] which generates a collection of intrinsic mode functions (IMFs) through a process termed *sifting*. Each of these intrinsic modes is a pure rotation in the complex plane, each with a properly defined frequency.

EMD is carried out as follows.

(i) Connect all the local maxima of the signal $I(t)$ through a cubic spline to get $I_{\max}(t)$. Similarly, obtain and connect all the local minima to get $I_{\min}(t)$.

(ii) Compute the mean of maxima and minima at each point and subtract it from the signal to get $\Delta I(t) \equiv I(t) - [I_{\max}(t)+I_{\min}(t)]/2$.

(iii) Verify that $\Delta I(t)$ corresponds to a proper rotation, else iterate steps (i) and (ii) until it does. The resulting signal is the first intrinsic mode, denoted by $C_1(t)$.

(iv) Subtract $C_1(t)$ from the signal $I(t) \equiv I(t) - C_1(t)$ and repeat steps (i)–(iii) on this new $I(t)$ to obtain second intrinsic mode $C_2(t)$.

(v) Continue this sifting procedure, until the mode $C_M(t)$ shows no apparent variation (for more details see Ref. [13]).

In the next section, we apply this analysis to time-series data from SNA dynamics.

III. STRANGE NONCHAOTIC DYNAMICS

We generate strange nonchaotic dynamics in the quasiperiodically driven Duffing oscillator [17],

$$\dot{x} = y,$$

$$\dot{y} = -0.1y + [1 + R(0.3\cos t + \cos \Omega t)]x - x^3, \tag{3}$$

where R is the forcing amplitude and the frequency Ω is the inverse of the golden mean ratio $(\sqrt{5}-1)/2$. Nominally these equations model buckled beam oscillations [18] and the system has been experimentally realized as a quasiperiodically driven magnetoelastic ribbon. Indeed, this provided one of the earliest demonstrations of strange nonchaotic dynamics in a physical system [19].

The autonomous system has fixed points (0,0) and $(\pm\sqrt{1.3R+1.0},0)$. A typical strange nonchaotic trajectory in the driven system is shown in Fig. 1(a) [20], and it is clear that the system oscillates around these three fixed points. Since there is no unique center of rotation, it is not possible to define the phase of oscillation in (x,y,z) coordinates and it is necessary to use the EMD.

Another system we consider is the Rössler oscillator [21] with quasiperiodic parameter modulation,

$$\dot{x} = -y - z,$$

$$\dot{y} = x + \frac{y}{10}[\alpha(\cos t + \cos \Omega t) + 1],$$

$$\dot{z} = \frac{1}{10} + z(x - 14), \tag{4}$$

where Ω is again taken to be the inverse golden mean ratio. In contrast to the Duffing system, there is a proper sense of rotation around the fixed point of the autonomous system, and thus a phase could be approximately defined as $\phi \approx \tan^{-1} y/x$. A typical trajectory of the system is shown in Fig. 1(b).

The IMF analysis is presented in Fig. 2 where the original signal along with the eight intrinsic modes generated from EMD process for the Duffing oscillator is plotted. Summing the eight IMFs essentially reconstructs the original signal with almost no residue [see Fig. 2(j)]. The phases $\phi(t)$ of these IMFs are obtained by Hilbert transformation, from which the average rotation frequencies are determined. The first mode has the largest frequency, and for higher modes, the frequencies decrease monotonically.

In Figs. 1(c) and 1(d), the analytic signal obtained by Hilbert transformation of the first IMF is plotted for trajectories of Duffing and Rössler oscillators: the rotation in the complex plane is now clearly evident. We also compute the largest Lyapunov exponent along with its variance for the above two dynamical systems as a function of respective parameters, and the results are shown in Fig. 3(a) (left panel)

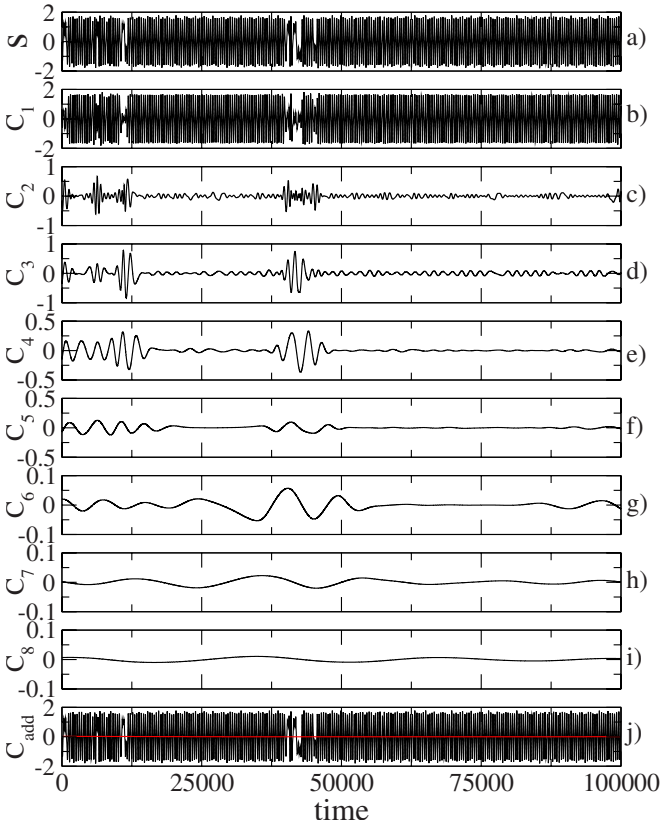

FIG. 2. (Color online) (a) Signal S for Duffing oscillator for R $=0.405$. (b)–(i) Eight successive IMFs (C_1-C_8) for the signal S. (j) Sum of the above eight IMFs (C_{add}) (black) with its residual (gray, red online) after EMD.

for Duffing and Fig. 3(b) (right panel) for Rössler systems. Earlier studies have used the variance in finite-time Lyapunov exponents as an order parameter for detecting the transition from torus to SNA [10]. The transitions from torus (T) to SNAs and from SNAs to chaos C are indicated by vertical dotted lines.

IV. RESULTS AND DISCUSSION

The Poincaré sections of typical SNAs and "nearby" chaotic attractors—as shown in Fig. 4, for example—can hardly be distinguished. Therefore, a measure which detects SNAs and distinguishes them from strange chaotic attractors in a system is desirable.

We apply the methodology outlined above to the two model systems to identify differences in the phase dynamics between SNAs and chaos. To do this, we generate several time series for different parameter values in both the systems. We applied EMD method to these signals (of typical length 2×10^5) to extract the two largest frequency modes from each time series. First the analytic signal was obtained by using the Hilbert transformation. From this, the phase and average instantaneous frequencies—say, ν_i—were determined. By repeating the procedure for $N=10^4$ uniformly distributed random initial conditions, we compute the average frequency, $\omega=\Sigma_{i=1}^{N}\nu_i$ and its variance, $\sigma_\omega^2=\omega-\Sigma_{i=1}^{N}\nu_i^2$, and

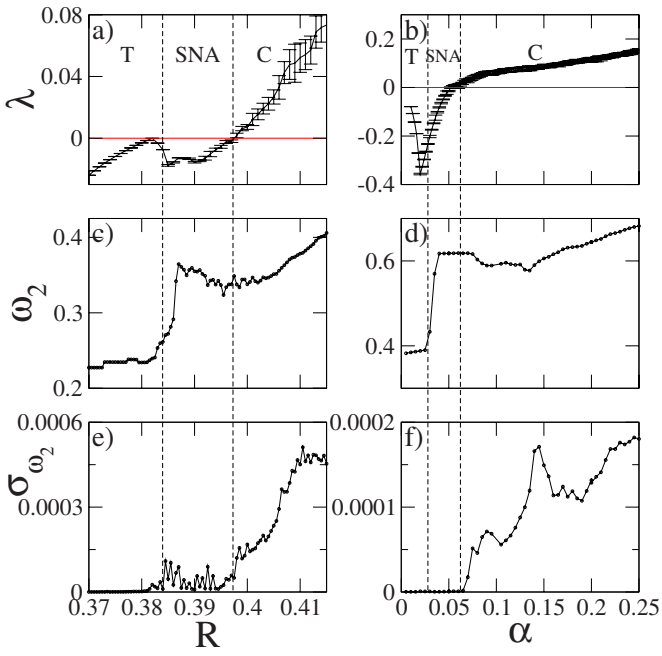

FIG. 3. (Color online) Left panel: forced Duffing oscillator. Right panel: Rössler system. (a),(b) Largest Lyapunov exponent λ and its variance (as error bars), (c),(d) second highest frequency IMF ω_2, and (e),(f) its variance $\sigma^2_{\omega_2}$.

examine their variation as a function of the parameters R and α in the two systems.

A. Transitions across SNAs

For both model systems, the first frequency (averaged) remains nearly constant in the nonchaotic regime and does not show any change at the transition from torus to SNAs. The variance of the first frequency shows a similar behavior and does not give any indication of this transition. In contrast, the second largest frequency shows a steep increase when the dynamics changes from torus to SNA in both the systems; see Figs. 3(c) and 3(d). In the Duffing oscillator, the rise is at $R\approx0.386$ and for the Rössler oscillator at $\alpha\approx0.028$, which are in agreement with the transition values determined from the variance in Lyapunov exponents as well [10]. The second mode is thus sensitive to the dynamical transition from torus to SNA.

At the SNA-to-chaos transition, the variance of the second-mode frequency shows a steep rise. This matches the point when the largest Lyapunov exponent becomes positive

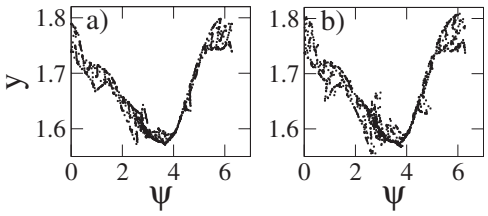

FIG. 4. Plot of $\psi(t)[\mathrm{mod}\,2\pi]$ vs y for the forced Duffing oscillator with (a) $R=0.395$ (SNA) and (b) $R=0.405$ (chaotic attractor).

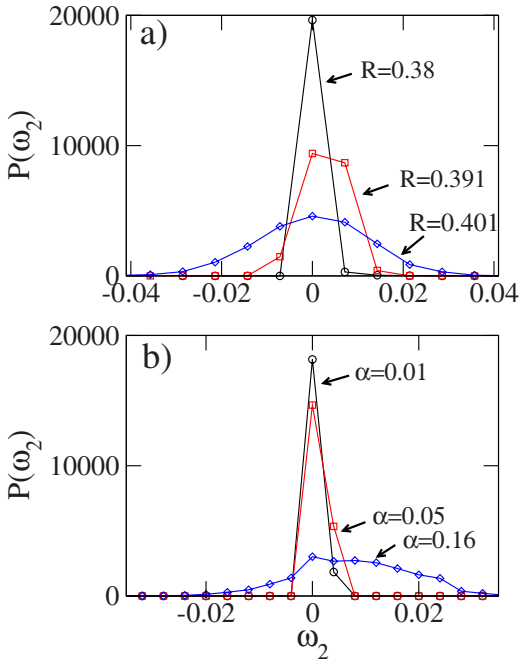

FIG. 5. (Color online) The probability distribution curves for the measured frequencies of the second IMF for the (a) Duffing oscillator and (b) Rössler oscillator. In each case, the distribution was computed from 20 000 different initial conditions.

as can be seen in Figs. 3(e) and 3(f). For the Duffing system this occurs at about $R \approx 0.398$ and for the Rössler oscillator at $\alpha \approx 0.06$.

B. Statistics of the frequency distributions

It has earlier been observed [11,16] that there is a large fluctuation in the frequency of the second IMF when the dynamics is chaotic as compared to the case where the motion is quasiperiodic. It would, therefore, be interesting to study the behavior of fluctuations in the frequency of the second IMF as the dynamics changes from regular to SNAs and from SNAs to chaos. The results are shown in Fig. 5 for both the forced Duffing and Rössler oscillators. In Fig. 5(a), $R=0.38$, 0.391, and 0.401 correspond to torus, SNA, and chaotic motions, respectively, for the Duffing system. The distribution is sharper in case of torus and SNA than it is for chaotic motion, offering a simple measure for distinguishing between them. Similar behavior is evident for the Rössler system as shown in Fig. 5(b) where $\alpha=0.01$, 0.05, and 0.16 correspond to torus, SNA, and chaotic motions, respectively.

C. Characteristics of SNAs and chaotic attractors

Along a trajectory, the local phase variable fluctuates as a function of time and depending on the nature of the dynamics—chaotic or nonchaotic—has a characteristic distribution. Figure 6 shows the fluctuations in phase for a SNA time series and a chaotic time series for the Rössler system. From this it is clear that the phase dynamics for SNAs is regular while that for chaos is irregular. To quantify these fluctuations, we calculate the Hurst exponent [22] of the time

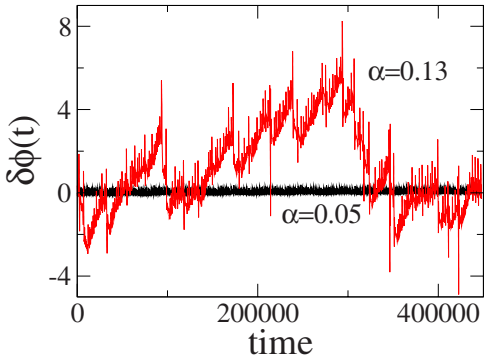

FIG. 6. (Color online) Phase fluctuations as a function of time for the modulated Rössler attractor with $\alpha=0.05$ (SNAs) and $\alpha=0.13$ (chaos).

series by a windowing method as follows [15].

To examine the nature of phase fluctuations in SNAs and chaos, we calculate the Hurst exponent [15,22,23] from the time series by generating a time series of 500 000 points corresponding to a given parameter value and applying the EMD method to sift out the largest frequency IMF from the time series. Then we derive its analytic signal by Hilbert transformation and obtain the phase at each time. The slope of this curve gives the average frequency. The fluctuations in phase about the average frequency are then plotted as a function of time.

We fix the window size N and find the absolute value of the difference in the phase fluctuation at time $t+N$ and t—namely, $|\Delta\phi_1(t)| \equiv |\delta\phi_1(t+N) - \delta\phi_1(t)|$—for each time t. We calculate the average of this quantity, $\langle|\Delta\phi_1(t)|\rangle$. By changing the window size N, we obtain the corresponding value of $\langle|\Delta\phi_1(t)|\rangle$ and plot $\log[\langle|\Delta\phi_1(t)|\rangle]$ versus $\log N$. (All logarithms are in base 10.) The Hurst exponent of the time series is the slope of the linear region of this curve. Figures 7(a) and 7(b) show the plot of $\log[\langle|\Delta\phi_1(t)|\rangle]$ versus $\log N$ for four different parameter values of the two systems corresponding to Duffing and Rössler systems, respectively. For shorter windows, SNAs and chaos behave similarly, initially rising linearly. The slope of the linear region is same for both SNAs and chaos, implying equal value of Hurst exponent. However, for longer windows the slope vanishes for SNAs, implying that the Hurst exponent is zero while for chaotic attractors the linear trend continues with same or different slope, implying a finite Hurst exponent.

In order to explain this different behavior between SNAs and chaos, we use finite-time Lyapunov exponent analysis which has been studied in a number of physical situations [24]. Although the Lyapunov exponents are global or asymptotic quantities, it is instructive to examine the distribution of Lyapunov exponents over finite-time segments (of length N) along a given trajectory. If the underlying attractor is chaotic but nonuniform, the local Lyapunov exponent (LE) can be negative within a finite-time interval. Similarly, on a nonchaotic trajectory the local LE can take positive values over finite-time intervals [25,26]. This gives a realization that local Lyapunov exponent statistics have characteristic forms depending on the nature of the attractors, and they may provide useful dynamical characterization of the state of a sys-

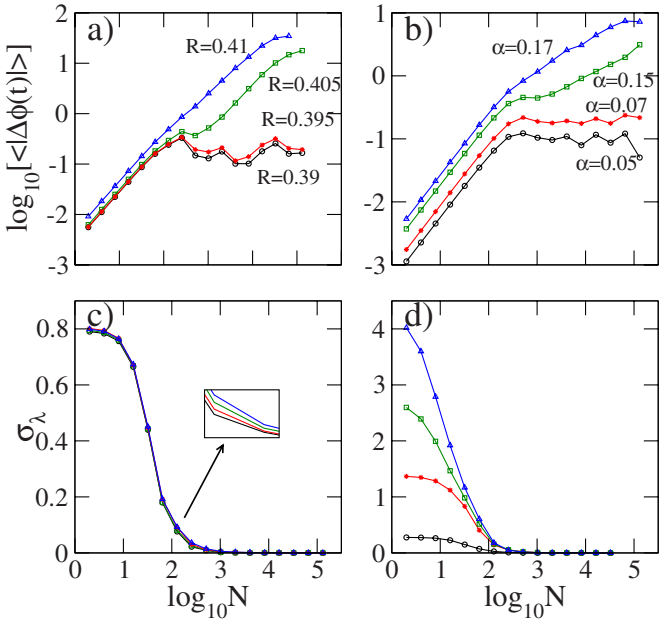

FIG. 7. (Color online) Left panel: forced duffing oscillator. Right panel: Rössler system. (a),(b) Plot of $\log_{10}\langle|\delta\phi|\rangle$ as a function of the window size N and (c),(d) the variance in the corresponding finite-time Lyapunov exponents.

tem. The plot of variance in finite time Lyapunov exponents of the two systems is shown in Figs. 7(c) and 7(d) for the parameter values of Figs. 7(a) and 7(b). The variance decreases as N increases and then becomes almost zero at $\log N \approx 2.5$, the point where crossover in scaling happens in a plot of $\log[\langle|\Delta\phi_1(t)|\rangle]$ versus $\log N$ for SNA dynamics.

Thus for SNAs, although the asymptotic Lyapunov exponent is negative, because of its fractal geometry, there are significant contributions from positive finite-time Lyapunov exponent as indicated by nonzero variance. For small time windows the local dynamics on SNAs is essentially chaotic, and this contributes to the initial linear rise in plot of $\log[\langle|\Delta\phi_1(t)|\rangle]$ versus $\log N$ for both SNAs and chaos. However, for sufficiently large time windows the variance in the finite-time Lyapunov exponent becomes zero and the curve shows saturation for SNAs since they are globally stable. For chaos, the curve keeps rising, indicating their global instability. This technique of studying the phase fluctuation dynamics can, therefore, be used as a diagnostic to detect whether the given time-series data is chaotic or from an SNA.

V. SUMMARY

In the present paper, we have applied an analytical signal analysis to study dynamical transitions in quasiperiodically driven nonlinear dynamical systems. The decomposition is on the basis of local characteristic time scales within the data and is, therefore, suitable when the data are nonstationary as well. Via the Hilbert transformation, the IMFs yield instantaneous frequencies, which makes it possible to examine the different characteristic time scales embedded in the data. This scheme is adaptive and therefore highly efficient. Results from two model systems suggest that the second largest frequency and its variance act as a good measure for the detection of the transition from tori to SNAs and from SNAs to chaos, respectively.

Strange nonchaotic attractors are an important example of stable nonperiodic motion, and there have been various suggestions as to their potential importance in natural systems [1,27] as well as in applications [28]. The ASA technique outlined here can be of considerable utility in the detection as well as characterization of experimental time series since there are few methods that can reliably compute negative Lyapunov exponents in aperiodic time-series data [29].

ACKNOWLEDGMENTS

K.G. would like to acknowledge support from the CSIR, India, and A.P. thanks the DST, India, for research support.

[1] A. Prasad, S. S. Negi, and R. Ramaswamy, Int. J. Bifurcation Chaos Appl. Sci. Eng. **11**, 291 (2001); A. Prasad, A. Nandi, and R. Ramaswamy, *ibid.* **17**, 2297 (2007).
[2] U. Feudel, S. Kuznetsov, and A. Pikovsky, *Strange Nonchaotic Attractors* (World Scientific, Singapore, 2006).
[3] An exceptional situation where chaos is not present is discussed in A. Prasad, R. Ramaswamy, I. I. Satija, and N. Shah, Phys. Rev. Lett. **83**, 4530 (1999).
[4] C. Grebogi, E. Ott, S. Pelikan, and J. A. Yorke, Physica D **13**, 261 (1984).
[5] A. Pikovsky and U. Feudel, Chaos **5**, 253 (1995).
[6] S. S. Negi, A. Prasad, and R. Ramaswamy, Physica D **145**, 1 (2000).
[7] G. Keller, Fund. Math. **151**, 139 (1996); J. Stark, Physica D **109**, 163 (1997); R. Sturman and J. Stark, Nonlinearity **13**, 113 (2000); B. R. Hunt and E. Ott, Phys. Rev. Lett. **87**, 254101 (2001).
[8] W. L. Ditto, M. L. Spano, H. T. Savage, S. N. Rauseo, J. Heagy, and E. Ott, Phys. Rev. Lett. **65**, 533 (1990); T. Zhou, F. Moss, and A. Bulsara, Phys. Rev. A **45**, 5394 (1992).
[9] G. Ruiz and P. Parmananda, Phys. Lett. A **367**, 478 (2007).
[10] A. Prasad, V. Mehra, and R. Ramaswamy, Phys. Rev. E **57**, 1576 (1998).
[11] Y. C. Lai and N. Ye, Int. J. Bifurcation Chaos Appl. Sci. Eng. **13**, 1383 (2003).
[12] E. J. Ngamga, A. Nandi, R. Ramaswamy, M. C. Romano, M. Thiel, and J. Kurths, Phys. Rev. E **75**, 036222 (2007).
[13] N. E. Huang, Z. Shen, S. R. Long, M. C. Wu, H. H. Shih, Q. Zheng, N. C. Yen, C. C. Tung, and H. H. Liu, Proc. R. Soc. London, Ser. A **454**, 903 (1998).
[14] D. Gabor, J. Inst. Electr. Eng. (London), Part III **93**, 429 (1946).
[15] W. S. Lam, W. Ray, P. N. Guzdar, and R. Roy, Phys. Rev. Lett. **94**, 010602 (2005).

[16] T. Yalcinkaya and Y. C. Lai, Phys. Rev. Lett. **79**, 3885 (1997).
[17] M. Lakshmanan and K. Murali, *Chaos in Nonlinear Oscillations: Synchronization and Controlling* (World Scientific, Singapore, 1996).
[18] J. F. Heagy and W. L. Ditto, J. Nonlinear Sci. **1**, 423 (1991).
[19] W. L. Ditto, S. Rauseo, R. Cawley, C. Grebogi, G. H. Hsu, E. Kostelich, E. Ott, H. T. Savage, R. Segnan, M. L. Spano, and J. A. Yorke, Phys. Rev. Lett. **63**, 923 (1989); H. T. Savage, W. L. Ditto, P. A. Braza, M. L. Spano, and W. C. Spring, J. Appl. Phys. **67**, 5619 (1990); H. T. Savage and M. L. Spano, *ibid.* **53**, 8092 (1982); H. T. Savage and C. Adler, J. Magn. Magn. Mater. **58**, 320 (1986).
[20] We use a Runge-Kutta fourth-order method to integrate the equations of motion with integration steps $\Delta t=0..02$ for the forced Duffing case and $\Delta t=0.01$ for Rössler oscillators.
[21] O. Rössler, Phys. Lett. **57A**, 397 (1976).
[22] A Hurst exponent $H=0.5$ implies that the signal is completely random while $H\neq 0.5$ is indicative of the fact that there are correlations in the data [23].
[23] H. E. Hurst, R. P. Black, and Y. M. Simaika, *Long-Term Storage: An Experimental Study* (Constable, London, 1965); P. Addison, *Fractal and Chaos* (IOP, Bristol, 1977).
[24] A. Prasad and R. Ramaswamy, Phys. Rev. E **60**, 2761 (1999), and references therein.
[25] A. Prasad and R. Ramaswamy, in *Nonlinear Dynamics: Integrability & Chaos*, edited by M. Daniel, R. Sahadevan, and K. Tamizhmani (Narosa, New Delhi, 1998), p. 227.
[26] Finite-time Lyapunov exponents on strange attractors usually behave like independent random variables with a distribution that obeys the central-limit theorem—namely, where the variance goes to zero asymptotically [24,25]; http://lanl.arxiv.org/abs/chao-dyn/9801021
[27] J. M. Shuai and D. M. Durand, Int. J. Bifurcation Chaos Appl. Sci. Eng. **13**, 251 (2003); A. Prasad, B. Biswal, and R. Ramaswamy, Phys. Rev. E **68**, 037201 (2003).
[28] R. Ramaswamy, Phys. Rev. E **56**, 7294 (1997).
[29] A. Ghosh and R. Ramaswamy, Phys. Rev. E **71**, 016224 (2005).